Journal of Sound and Vibration (1999) **223**(1), 1–21
Article No. jsvi.1998.2062, available online at http://www.idealibrary.com on IDEAL®

DESIGN OF OPTIMUM SUPPORT PARAMETERS FOR MINIMUM ROTOR RESPONSE AND MAXIMUM STABILITY LIMIT

K. C. PANDA AND J. K. DUTT
Department of Mechanical Engineering, Indian Institute of Technology, Kharagpur 721 302, *India*

(*Received* 13 *November* 1996, *and in final form* 2 *November* 1998)

Viscoelastic polymeric materials provide good support elements to rotor shaft systems by virtue of their efficiency in dissipating vibratory energy. The in-phase stiffness and loss factor for such materials also change with the frequency of excitation they are subjected to. In this paper frequency dependent characteristics of the polymeric supports have been found by simultaneously minimizing the unbalanced response and maximizing the stability limit speed. This process yields better support characteristics than those obtained by minimizing unbalance response alone. Optimum characteristics have been found for the rotor shaft system mounted on (a) rolling element bearings and (b) plain cylindrical journal bearings at the ends having polymeric supports. The effects of viscous internal damping in the shaft, support mass and gyroscopic effect due to non-symmetrical location of the disc have been considered in the analysis. A procedure of controlling the slope of the support characteristics versus frequency of excitation has been used and found to be very suitable for obtaining feasible support characteristics. Examples have been presented to justify the above conclusions.

1. INTRODUCTION

Two major causes for excessive transverse vibration of a rotor–shaft system are (i) the unbalance in the rotor and (ii) the loss of stability of the rotor–shaft system. The former generates sinusoidal forces of excitation which are responsible for excessive vibration at resonance, while the latter occurs above a certain speed called the "Stability Limit Speed" when a slight perturbation grows with time, aided by the energy of rotation of the rotor. Hence, smooth operation of the rotor–shaft system demands minimum Unbalance Response (UBR) and a Stability Limit Speed (SLS) much higher than the operating speed of the rotor. Flexible damped supports discussed in references [1–4] were observed to reduce the UBR and increase the SLS. Researchers also reported suitable values of the support parameters that offer low UBR and high SLS. A notable work by Pilkey *et al.* [5] applied the Linear Programming Technique to minimize the UBR. No attention was, however, paid to finding the SLS. A

0022–460X/99/210001 + 21 $30.00/0

noteworthy work reported by Bhat *et al.* [6] used an optimization technique to find the optimum dimensions of a plain cylindrical journal bearing and the viscosity of the oil to achieve minimum UBR. Barret *et al.* [7] reported optimum support damping to minimize the UBR and maximize the SLS in the vicinity of the first critical speed of a rotor–shaft system. The effects of support mass and polymeric support materials were, however, not considered. By virtue of the ability of dissipating vibratory energy efficiently, polymeric materials [8] have been used in many mechanical systems as vibration absorbers having many operational advantages. Dutt and Nakra [9] reported improvements in SLS of rotor–shaft systems having polymeric supports in comparison with conventional flexible damped supports and observed the existence of optimum values of polymeric support parameters to achieve maximum SLS. When subjected to sinusoidal excitations, polymeric materials exhibit in-phase stiffness and loss factor both of which vary with the frequency of excitation. Dutt and Nakra [10] utilized this property of the polymeric materials and predicted suitable frequency dependent support characteristics (in terms of in-phase stiffness and loss factor) to avoid resonance due to unbalance excitation for a rotor–shaft system with single symmetrically placed rotor disc. The procedure followed in reference [10] is difficult to apply to continuous multi-rotor multi support systems.

References discussed so far, did not assess the SLS, a very important index of rotor operation, while minimizing the UBR. The idea of Barret *et al.* [7] has been furthered here to predict suitable frequency dependent support characteristics which keep the SLS of the system well above the operating speed of the rotor while minimizing the UBR. The system considered in this work comprises a single unbalanced rotor disc placed on a mass-less elastic rotor–shaft mounted on bearings at the ends supported on polymeric supports. Effects of support mass, frequency dependent properties of the supports, viscous internal damping in the shaft and the gyroscopic effect have been considered in the analysis. Effects of rolling element and plain cylindrical journal bearings have been studied separately in Cases I and II. Case II differs from Case I in the sense that in Case II, the destabilizing forces arise due to the oil film in addition to the rotary internal damping force, the only source of destabilizing force in Case I. A detailed parametric study to show the effects of varying system parameters on the SLS, and the optimum support characteristics have been presented.

2. EQUATIONS OF MOTION

The system is schematically shown in Figure 1(a). The rotor disc of mass M_2 is placed assymetrically along the shaft. I_p and I_t denote respectively the polar and transverse mass moments of inertia of the rotor disc. The bearings are modelled to have, in general, eight stiffness and damping coefficients. (K_{xx}, C_{xx}) and (K_{yy}, C_{yy}) denote the direct stiffness and damping coefficients in the X and Y directions respectively. (K_{yx}, C_{yx}) and (K_{xy}, C_{xy}) denote the cross coupled stiffness and damping coefficients along the X and Y directions. The four-element model [9] shown in Figure 1(b) represents the polymeric support. K_1 and

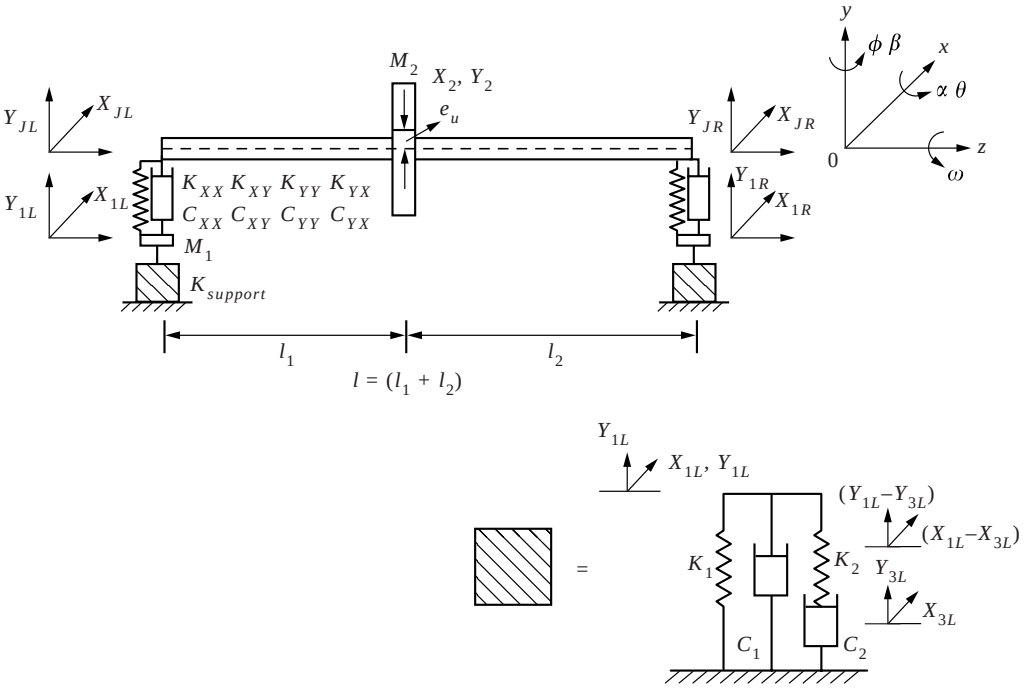

Figure 1. System diagram.

C_1 denote primary support stiffness and damping coefficients while K_2 and C_2 denote respectively the secondary support stiffness and damping coefficients.

The expression given below for kinetic energy T has been obtained from the respective expression in reference [11] after adding the underlined terms due to each support mass.

$$T = 1/2[M_2\dot{X}_2^2 + M_2\dot{Y}_2^2 + I_p\omega^2 + I_t\dot{\theta}^2 + I_t\dot{\phi}^2 + 2I_p\omega\dot{\phi}\theta + \underline{M_1\dot{X}_{1L}^2 + M_1\dot{Y}_{1L}^2 + M_1\dot{X}_{1R}^2 + M_1\dot{Y}_{1R}^2}]. \quad (1)$$

The expression given below for Strain energy V has been obtained from the respective expression in reference [11] after adding the underlined terms due to the stiffnesses of bearings and supports.

$$V = 1/2[K_sX_s^2 + K_sY_s^2 + C_{22}(\theta-\alpha)^2 + C_{22}(\phi-\beta)^2 - C_{12}(\theta-\alpha)Y_s - C(\phi-\beta)X_s$$
$$\underline{+(K_{xx})_LX_{JL}^2 + (K_{yy})_LY_{JL}^2 + (K_{xx})_RX_{JR}^2 + (K_{yy})_RY_{JR}^2 + 2\{((K_{xy})_LY_{JL})X_{JL}}$$
$$\underline{+((K_{yx})_LX_{JL})Y_{JL} + ((K_{xy})_RY_{JR})X_{JR} + ((K_{yx})_RX_{JR})Y_{JR}\} + K_1(X_{1L}^2}$$

$$+Y_{1L}^2 + X_{1R}^2 + Y_{1R}^2) + K_2\{(X_{1L} - X_{3L})^2 + (Y_{1L} - Y_{3L})^2 + (X_{1R} - X_{3R})^2 + (Y_{1R} - Y_{3R})^2\}], \tag{2}$$

where the subscripts L and R denote the left and right sides, respectively. The stiffnesses of the shaft at the location of the disc are denoted by K_s, C_{12} and C_{22} the expressions of which are given below.

K_s (force/deflection) $= K^*(e_1^2 + e_2^2 - e_1e_2)/e_1e_2$, C_{12} (force/angular deflection or moment/deflection) $= K^*l(e_2 - e_2)$ and C_{22} (moment/angular deflection) $= K^*l^2e_1e_2$, where $e_i = l_1/l$, $e_2 = l_2/l$ and $K^* = 3EI/l_1^2l_2^2$, E and I being the Young's modulus of the material of the shaft and area moment of inertia of the cross section of the shaft, respectively. Simply supported end conditions were considered for the calculations of the stiffnesses.

The expressions of α, β, X_s, Y_s are given below

$$\alpha = (Y_{JR} + Y_{1R} - Y_{JL} - Y_{1L})/l, \tag{3a}$$

$$\beta = (X_{JR} + X_{1R} - X_{JL} - X_{1L})/l, \tag{3b}$$

$$X_s = X_2 - (X_{JL} + X_{1L})e_2 - (X_{JR} + X_{1R})e_1, \tag{3c}$$

$$Y_s = Y_2 - (Y_{JL} + Y_{1L})e_2 - (Y_{JR} + Y_{1R})e_1. \tag{3d}$$

The expression given below for dissipated energy D has been obtained from the respective expression in reference [2] after adding the underlined terms due to the damping in bearings and supports.

$$D = C_i[(\dot{X}_s^2 + \dot{Y}_s^2)/2 + \omega(Y_s\dot{X}_s - X_s\dot{Y}_s)] + \underline{\tfrac{1}{2}C_1[\dot{X}_{1L}^2 + \dot{Y}_{1L}^2 + \dot{X}_{1R}^2 + \dot{Y}_{1R}^2]}$$
$$\underline{+\tfrac{1}{2}C_2[\dot{X}_{3L}^2 + \dot{Y}_{3L}^2 + \dot{X}_{3R}^2 + \dot{Y}_{3R}^2] + \tfrac{1}{2}[2\{(C_{xy})_L\dot{Y}_{JL}\dot{X}_{JL} + (C_{yx})_L\dot{X}_{JL}\dot{Y}_{JL}}$$
$$\underline{+(C_{xy})_R\dot{Y}_{JR}\dot{X}_{JR} + (C_{yx})_R\dot{X}_{JR}\dot{Y}_{JR}\} + (C_{xx})_L\dot{X}_{JL}^2 + (C_{yy})_L\dot{Y}_{JL}^2}$$
$$\underline{+(C_{xx})_R\dot{X}_{JR}^2 + (C_{yy})_R\dot{Y}_{JR}^2]}. \tag{4}$$

Substituting equations (3) into equations (1), (2) and (4) and using Lagrange's equations in generalized co-ordinates, 16 unforced equations of motion are obtained and given in Appendix A.

3. UNBALANCE RESPONSE AND STABILITY LIMIT SPEED

3.1. CASE I—SYSTEM WITH ROLLING ELEMENT BEARINGS

The rolling element bearings are modelled to have only direct stiffness coefficients equal in magnitude in both x and y directions. Hence, the equations of motion for this system can be obtained from those given in Appendix A, by making the following substitutions:

$$(K_{xx})_L = (K_{yy})_L = (K_b),\ (K_{xy})_L = (K_{yx})_L = (C_{xx})_L = (C_{xy})_L = (C_{yx})_L = (C_{yy})_L = 0,$$
$$(K_{xx})_R = (K_{yy})_R = (K_b),\ (K_{xy})_R = (K_{yx})_R = (C_{xx})_R = (C_{xy})_R = (C_{yx})_R = (C_{yy})_R = 0.$$

For checking the correctness, we put $C_i = 0$ and ignoring the support mass, the equations are seen to be identical to those in reference [11]. Again, the equations can be reduced to those in reference [3] if the gyroscopic effect is ignored and the rotor is assumed to be in the middle of the shaft.

3.1.1. *Unbalance response*

Unbalance response of the rotor has been determined by solving the forced equations of motion. The components of the unbalance force along X and Y are $M_2 e_u \omega^2 \cos(\omega t)$ and $M_2 e_u \omega^2 \sin(\omega t)$ where e_u is the eccentricity at rotor disc and "t" is the time in seconds. Considering the forces due to unbalance the equations of motion obtained from Appendix A can be written in the form:

$$[M\{\ddot{\mathbf{Q}}\} + [C]\{\dot{\mathbf{Q}}\} + [K]\{\mathbf{Q}\} = \{\mathbf{F}\}, \tag{5}$$

where $[M]$, $[C]$ and $[K]$ are the mass, damping and stiffness matrices, respectively. The force and displacement vectors $\{\mathbf{F}\}$, $\{\mathbf{Q}\}$ are

$$\{\mathbf{F}\} = [M_2 e_u \omega^2 \cos(\omega t),\ M_2 e_u w^2 \sin(\omega t),\ 0,\ 0,\ 0,\ 0,\ 0,\ 0,\ 0,\ 0,\ 0,\ 0,\ 0,\ 0,\ 0,\ 0]^T$$

$$\{\mathbf{Q}\} = [X_2,\ Y_2,\ X_{JL},\ Y_{JL},\ X_{JR},\ Y_{JR},\ X_{1L},\ Y_{1L},\ X_{1R},\ Y_{1R},\ X_{3L},\ Y_{3L},\ X_{3R},\ Y_{3R},\ \phi,\ \theta]^T.$$

The force vector can also be written as $\{\mathbf{F}\} = \{\mathbf{f}\}e^{i\omega t}$. Assuming harmonic solutions of the form $Q_i = q_i e^{i\omega t}$, where Q_i is the ith element of $\{\mathbf{Q}\}$, the equations of motion can be represented as

$$[-\omega^2[M] + i\omega[C] + [K]]\{\mathbf{q}\} = \{\mathbf{f}\}. \tag{6}$$

Using the non-dimensional parameters: $\delta = \omega/\omega_n$, $\omega_n = \sqrt{K^*/M_2}$, $R = I_p/I_t$, η, $\alpha_1 = M_1/M_2$, $\beta_b = K_b/K^*$, $\zeta_i = C_i/C_c$, where $C_c = 2M_2\omega_n$, $\beta_1 = K_1/K^*$, $\beta_2 = K_2/K^*$, $\zeta_1 = C_1/C_c$, $\zeta_2 = C_2/C_c$, $\beta_{xx} = K_{xx}/K^*$, $\beta_{xy} = K_{xy}/K^*$, $\beta_{yx} = K_{yx}/K^*$, $\beta_{yy} = K_{yy}/K^*$, $\zeta_{xx} = C_{xx}/C_c$, $\zeta_{xy} = C_{xy}/C_c$, $\zeta_{yx} = C_{yx}/C_c$, $\zeta_{yy} = C_{yy}/C_c$, the *forced* non-dimensional equations of motion of the rotor–shaft system can be written, as given in Appendix B, and can be expressed in the form:

$$[A][\{\mathbf{q}\} = \{\mathbf{f}\} \tag{7}$$

Now the unbalance response can be calculated as

$$z_2 = [\mathrm{Real}(x_2 e^{i\omega t}) + i\,\mathrm{Real}(y_2 e^{i\omega t})], \tag{8}$$

where z_2 is a complex quantity. The non-dimensional unbalance response amplitude is expressed as

$$\mathrm{RD} = |z_2|/e_u. \tag{9}$$

Solving equation (7) for x_2 and y_2 and using equations (8) and (9) the unbalance response amplitude RD can be found out.

3.1.2. *Stability Limit*

To find the stability limit speed of the system, equation (5) is written with right side forces equated to zero and can be expressed in the form:

$$\begin{bmatrix} 0 & M \\ M & 0 \end{bmatrix} \begin{Bmatrix} \ddot{q} \\ \dot{q} \end{Bmatrix} + \begin{bmatrix} -M & 0 \\ C & K \end{bmatrix} \begin{Bmatrix} \dot{q} \\ q \end{Bmatrix} = \{\mathbf{0}\}$$

or

$$[A1]\{\dot{\mathbf{u}}\} + [A2]\{\mathbf{u}\} = \{\mathbf{0}\}, \tag{10}$$

where

$$\begin{Bmatrix} \dot{q} \\ q \end{Bmatrix} = \{\mathbf{u}\} \quad \text{and} \quad \begin{Bmatrix} \ddot{q} \\ \dot{q} \end{Bmatrix} = \{\dot{\mathbf{u}}\}.$$

After converting the equations into the form as in equation (10) the stability limit speed was found by examining the sign of the real part of the eigenvalues, which are complex in general, for each step of increment of speed, using the EISPACK subroutine [7]. The non-dimensional stability limit speed is represented by DLIMIT.

DLIMIT = stability limit speed/speed of the rotor.

3.2. CASE II—SYSTEM WITH PLAIN CYLINDRICAL JOURNAL BEARINGS

For this case the rotor disc is considered to be in the middle of the shaft. The equations of motion have been found by substituting the following into the equations of motion given in Appendix A:

$$(K_{xx})_L = (K_{xx})_R = K_{xx},\ (C_{xx})_L = (C_{xx})_R = C_{xx},\ X_{1L} = X_{1R} = X_1,$$
$$Y_{1L} = Y_{1R} = Y_1,\ X_{jL} = X_{jR} = X_j,\ Y_{jL} = Y_{jR} = Y_j,\ X_{3L} = X_{3R} = X_3,$$
$$Y_{3L} = Y_{3R} = Y_3,\ C_{12} = C_{22} = \alpha = \beta = 0 \quad \text{and} \quad e_1 = e_2 = 0{\cdot}5.$$

After the above substitutions the total number of equations will reduce to eight. The expressions for K_{xx}, K_{xy}, K_{yy}, K_{yx} and C_{xx}, C_{xy}, C_{yy}, C_{yx} in terms of Sommerfeld number were taken from reference [13]. The unbalance response and stability limit speed of the system can be found in the fashion followed in Case I.

4. OPTIMIZATION

After determining the unbalance response and stability limit speed as functions of non-dimensional support parameters β_1, β_2, ζ_1, ζ_2, optimization has been carried out in order to predict the optimum support characteristics i.e., K_{sn} and η, which are given below

$$K_{sn} = \left[\frac{\beta_1\beta_2 + 4\delta^2\zeta_2^2(\beta_1 + \beta_2)}{\beta_2^2 + 4\delta^2\zeta_2^2)}\right], \tag{11}$$

$$\eta = \frac{2\delta[\beta_2^2\zeta_1 + \beta_2^2\zeta_2 + 4\zeta_1\zeta_2\delta^2]}{[\beta_1\beta_2^2 + 4\zeta_2^2\delta^2(\beta_1 + \beta_2)]}. \tag{12}$$

Two schemes of optimization have been used.

Scheme I

Objective = minimize (RD)

Constraints: (a) constraints for support parameters; (b) constraints for space restrictions and other system constraints.

Scheme II

Objective = minimize (RD-DLIMIT)

Constraints: (a) constraints for support parameters; (b) constraints for space restrictions and other system constraints.

η is the loss factor of the viscoelastic support. The characteristics of viscoelastic materials are given in reference [14]. It is found that the inphase stiffness increases uniformly and monotonically with frequency of excitation while the variation of loss factor with excitation frequency is uniform. Again it is observed that generally the maximum value of the loss factor is $\leqslant 1$. Hence, the support constraint used in this work is $\eta \leqslant 1$. However, no constraints on space restrictions or other system constraints have been considered in this work. They can definitely be taken care of under the schemes proposed. The objective function has been optimised by an optimization subroutine which optimizes the function by the gradient method [15]. The objective function is optimized for each step wise increment of the speed of rotation, to predict values for support parameters for that speed.

5. IMPORTANCE OF SLOPE CONTROL

5.1. EXAMPLE

Figures 2(a–d) show respectively the plots of (RD and DLIMIT), (β_1 and β_2), (ζ_1 and ζ_2) and (K_{sn} and η) drawn against δ obtained after carrying out the optimization process described under Scheme II, for a rotor–shaft system mounted on rolling element bearings at the ends supported on polymeric supports. Figures 3(a–d) show similar plots for the system with plain cylindrical journal bearings. It is noticed that the plots of (K_{sn} and η) include sudden changes in slopes. It is obvious that the support characteristics are difficult, if not impossible, to generate by using any polymeric material for which the characteristics are smooth. Therefore, a slope control technique, as described below, has been used to restrain the slope of the support parameters within specified bounds to obtain smooth support characteristics.

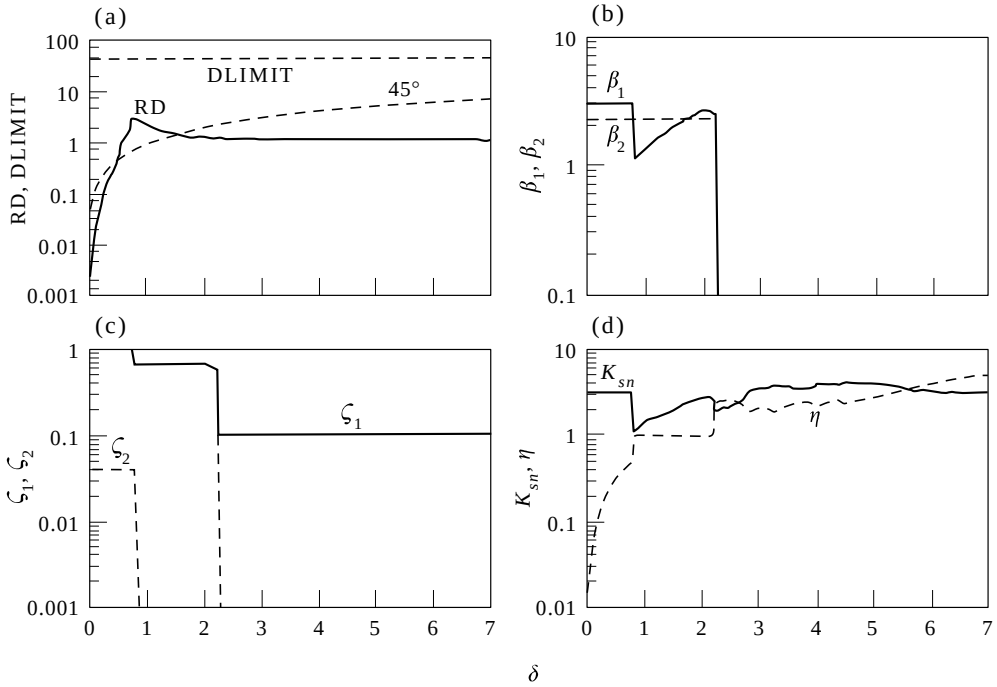

Figure 2. (a) Minimization of RD and maximization of DLIMIT, with out slope control, for system with rolling element bearings; $\alpha_1 = 0{\cdot}4$, $\beta_b = 8$, $\zeta_i = 0{\cdot}05$, $e_1 = 0{\cdot}1$. (b) Variation of β_1 and β_2 w.r.t δ. (c) Variation of ζ_1 and ζ_2 w.r.t. δ. (d) Variation of K_{sn} and η w.r.t δ.

5.2. SLOPE CONTROL

Restriction on the change of slope was imposed on the variations of the support parameters β_1, β_2, ζ_1, ζ_2, against δ such that the slope of each at any value of δ remains within 0° to 20°, a value chosen tacitly as the upper bound. To start with, the values of support parameters have been taken to be at the respective lower limits. An optimization process has been carried out to find the support parameters abiding by the slope restrictions for subsequent increment of speeds.

6. RESULTS AND DISCUSSION

6.1. SYSTEMS WITH ROLLING ELEMENT BEARINGS

6.1.1. *Parametric study of stability limit speed*

To start with, a parametric analysis for the stability limit speed has been presented to show the effect of different non-dimensional system parameters on the stability limit speed. A set of values for the parameters has been chosen. One parameter has been selected at a time and its value has been varied keeping the value of the others fixed.

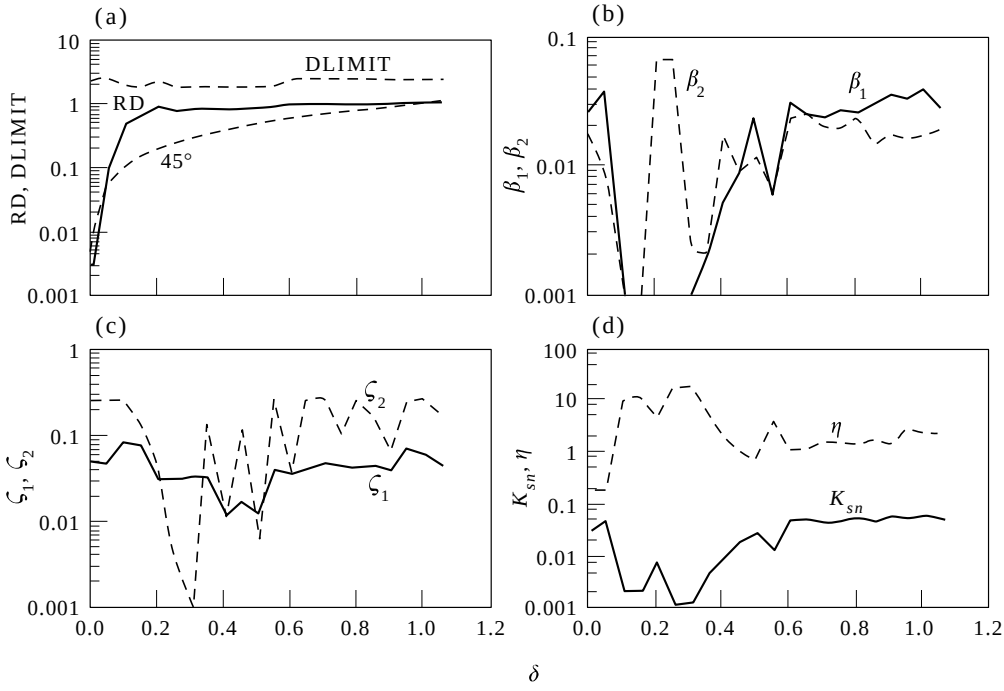

Figure 3 (a) Minimization of RD and maximization of DLIMIT, without slope control, for system with plain cylindrical journal bearings; $\alpha_1 = 0{\cdot}1$, $\zeta_i = 0{\cdot}01$, $e_1 = 0{\cdot}5$. (b) Variation of β_1 and β_2 w.r.t.. δ. (c) Variation of ζ_1 and ζ_2 w.r.t. δ. (d) Variation of K_{sn} and η w.r.t. δ.

Figure 4 shows the variation of non-dimensional stability limit speed (DLIMIT) of the system with rolling element bearings at the ends with respect to the non-dimensional location of the rotor disc on the shaft (e_1). A non-central location of the disc gives rise to the gyroscopic couple as the slope of the rotor shaft at the location of the rotor disc changes. The gyroscopic couple results in stiffening of the shaft. Hence it becomes difficult to change the slope of the shaft at the location of the disc and the stability limit speed increases. It is observed

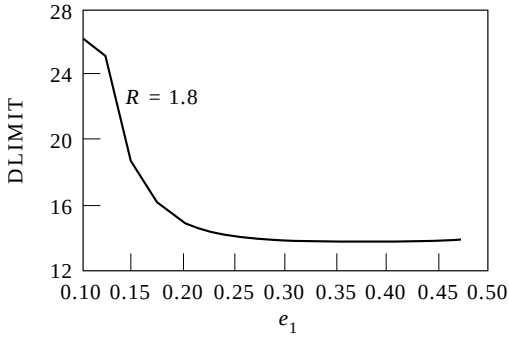

Figure 4 Variation of stability limit w.r.t. e_1; $\alpha_1 = 0{\cdot}4$, $\beta_b = 4$, $\beta_1 = 0{\cdot}4$, $\beta_2 = 0{\cdot}1$, $\zeta_i = 0{\cdot}005$, $\zeta_1 = 0{\cdot}015$, $\zeta_2 = 0{\cdot}02$.

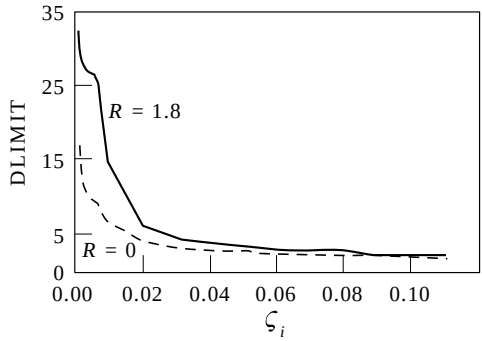

Figure 5. Variation of stability limit w.r.t. ζ_i; $\alpha_1 = 0{\cdot}4$, $\beta_b = 4$, $\beta_1 = 0{\cdot}4$, $\beta_2 = 0{\cdot}1$, $\zeta_1 = 0{\cdot}015$, $\zeta_2 = 0{\cdot}02$, $e_1 = 0{\cdot}1$.

from the figure that the stability limit speed diminishes progressively as the disc is moved towards the center and the gyroscopic couple is reduced.

Two curves have been drawn in each figure from Figure 5 to Figure 11. The curve in the solid line (—) has been drawn taking into account the gyroscopic couple, while the other in dotted lines (...) has been drawn after ignoring the gyroscopic couple introduced by the disc which is still placed non-centrally.

Figure 5 shows the variation of DLIMIT of the rotor–shaft system with respect to different values of ζ_i of the shaft. It is well established [10, 11] that the internal damping in the shaft reduces the stability limit speed. The same is true in this case. Again it is observed that the gyroscopic couple helps in stabilizing the system.

Figure 6, shows the variation of DLIMIT with respect to different values of support mass ratio (α_1). The heavier the support, the more the dynamic inertia load on the system which is destabilized faster. Still the gyroscopic couple provides a higher stability limit speed.

Figures 7 and 8 show the variation of DLIMIT with respect to different values of non-dimensional primary support stiffness and damping β_1 and ζ_1. The primary support stiffness and damping play important roles in deciding the

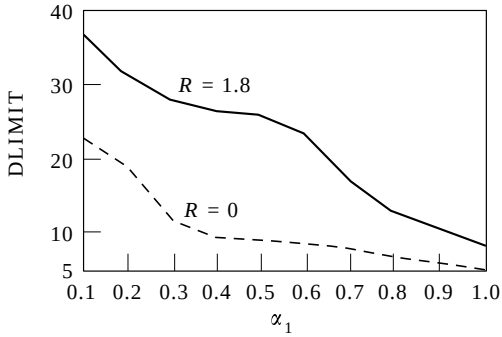

Figure 6. Variation of stability limit w.r.t. α_1; $\beta_b = 4$, $\beta_1 = 0{\cdot}4$, $\beta_2 = 0{\cdot}1$, $\zeta_i = 0{\cdot}005$, $\zeta_1 = 0{\cdot}015$, $\zeta_2 = 0{\cdot}02$, $e_1 = 0{\cdot}1$.

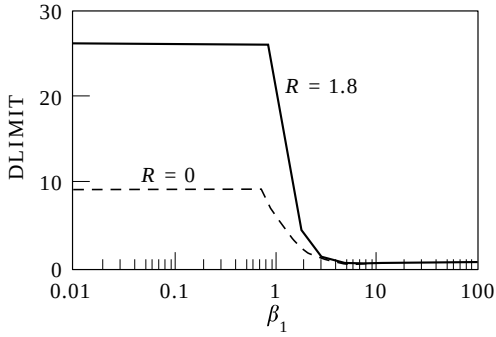

Figure 7. Variation of stability limit w.r.t. β_1; $\alpha_1 = 0{\cdot}4$, $\beta_b = 4$, $\beta_2 = 0{\cdot}1$, $\zeta_i = 0{\cdot}005$, $\zeta_1 = 0{\cdot}015$, $\zeta_2 = 0{\cdot}02$, $e_1 = 0{\cdot}1$.

stability limit speed. It is well known that support damping increases the stability limit speed, but it happens only when the support gets deflected. If either the primary support stiffness or the primary support damping assumes a very high value, the support tends to be rigid and hence the stabilizing effects of the support damping are not obtained. Therefore, it is observed from the figures, as well as supported by references [10, 11], that very high values of β_1 and ζ_1 lowers the stability limit speed. There remains optimum values for each of these parameters corresponding to the maximum stability limit speed. It is also observed that the gyroscopic couple postpones the destabilizing effects.

Figures 9 and 10 show the variation of DLIMIT with respect to different non-dimensional values of secondary support stiffness and damping β_2 and ζ_2. When either secondary support stiffness or secondary support damping becomes very high, the support can still be deflected. On the one hand when β_2 becomes very high the deflection of the support includes the effects of secondary support damping, and on the other hand, when ζ_2 is very high, the effects of secondary support stiffness is included. Out of the two cases, when the stabilizing effect of secondary support damping is included, the dissipation of energy becomes more efficient and hence a higher stability limit speed is obtained in comparison to the case when the effects of secondary support stiffness is included.

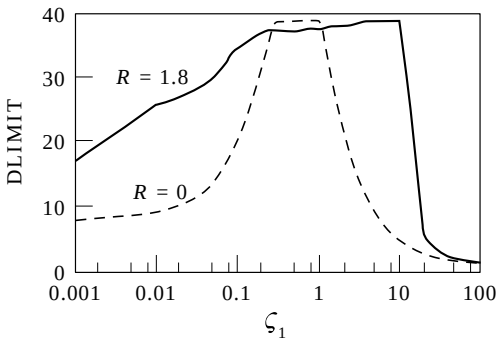

Figure 8. Variation of stability limit w.r.t. ζ_1; $\alpha_1 = 0{\cdot}4$, $\beta_b = 4$, $\beta_1 = 0{\cdot}4$, $\beta_2 = 0{\cdot}1$, $\zeta_i = 0{\cdot}005$, $\zeta_2 = 0{\cdot}02$, $e_1 = 0{\cdot}1$.

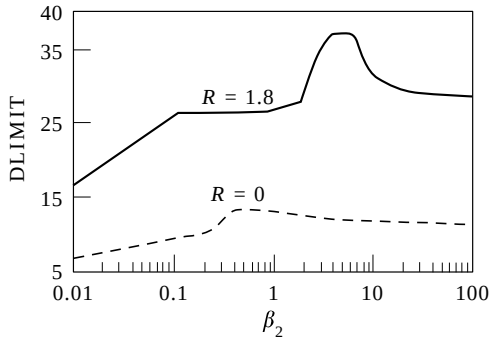

Figure 9. Variation of stability limit w.r.t. β_2; $\alpha_1 = 0{\cdot}4$, $\beta_b = 4$, $\beta_1 = 0{\cdot}4$, $\zeta_i = 0{\cdot}005$, $\zeta_1 = 0{\cdot}015$, $\zeta_2 = 0{\cdot}02$, $e_1 = 0{\cdot}1$.

Figure 11 shows the variation of DLIMIT with respect to non-dimensional bearing stiffness β_b. No clear physical justification can be given for such variation but (a) there exists an optimum value for each of these parameters for maximum stability limit, and (b) gyroscopic effect helps to maintain the stability. Hence, there is an optimum combination of support parameters for obtaining the maximum stability limit speed.

6.1.2. *Optimization results*

In this section the optimum frequency dependent support characteristics and the corresponding RD and DLIMIT obtained by using the optimization procedures described under Schemes I and II are presented.

Figures 12 and 13 show the variations of RD and DLIMIT with respect to δ for Schemes I and II, respectively with the concept of slope control applied to the variation of support characteristics. Figures 14 and 15 present the respective support characteristics. Comparing Figures 12 and 13, it is observed that Scheme II undoubtedly improves the stability limit speed in comparison to Scheme I but the effect of Scheme II is marginal. It is also observed that the support

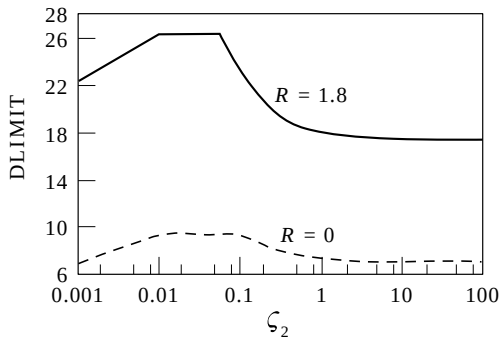

Figure 10. Variation of stability limit w.r.t. ζ_2; $\alpha_1 = 0{\cdot}4$, $\beta_b = 4$, $\beta_1 = 0{\cdot}4$, $\beta_2 = 0{\cdot}1$, $\zeta_i = 0{\cdot}005$, $\zeta_1 = 0{\cdot}015$, $e_1 = 0{\cdot}1$.

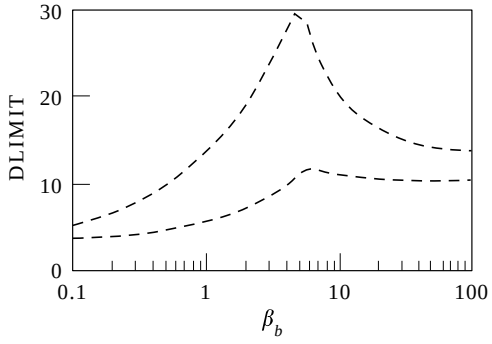

Figure 11. Variation of stability limit w.r.t. β_b; $\alpha_1 = 0{\cdot}4$, $\beta_1 = 0{\cdot}4$, $\beta_2 = 0{\cdot}1$, $\zeta_i = 0{\cdot}005$, $\zeta_1 = 0{\cdot}015$, $\zeta_2 = 0{\cdot}02$, $e_1 = 0{\cdot}1$.

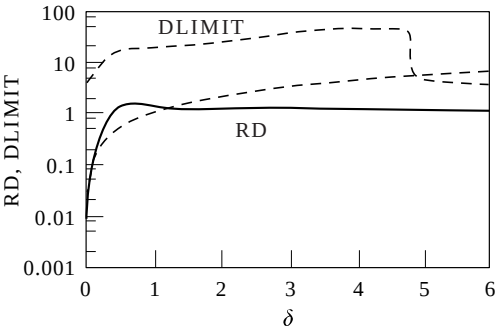

Figure 12. Variation of RD and DLIMIT w.r.t δ when RD is minimized, with slope control.

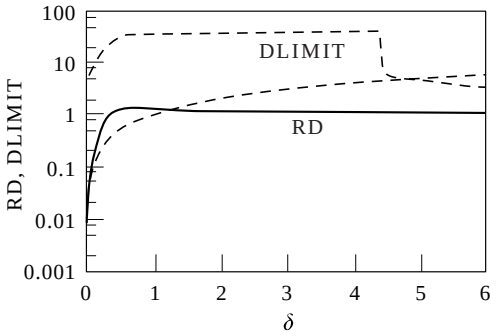

Figure 13. Variation of RD and DLIMIT w.r.t δ when RD is minimized and DLIMIT is maximized, with slope control.

characteristics are fairly smooth and do not involve any sudden change. This is the advantage of using the slope control technique.

6.2. SYSTEM WITH PLAIN CYLINDRICAL JOURNAL BEARINGS

When the rotor–shaft system is mounted on plain cylindrical journal bearings at the ends, destabilizing forces arise due to the fluid film in the bearings, in addition to the internal damping forces caused by the deflection and rotation of

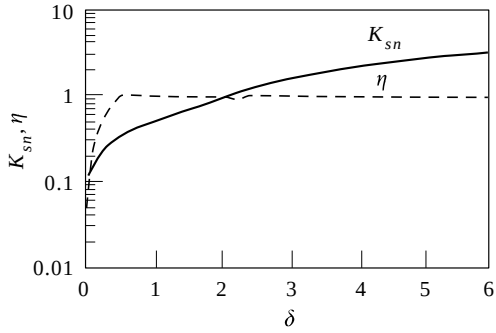

Figure 14. Variation of K_{sn} and η w.r.t. δ when RD is minimized.

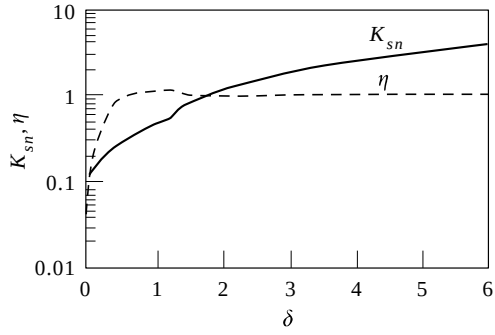

Figure 15. Variation of K_{sn} and η w.r.t. δ when RD is minimized and DLIMIT is maximized.

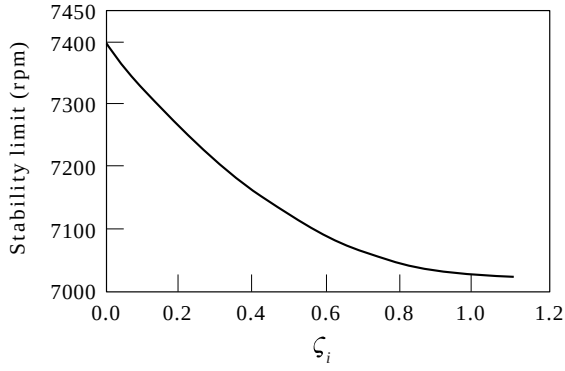

Figure 16. Variation of DLIMIT w.r.t ζ_i. $\zeta_1 = 0{\cdot}1$, $\zeta_2 = 0{\cdot}2$, $\alpha_1 = 0{\cdot}1$, $\beta_1 = 0{\cdot}2$, $\beta_2 = 0{\cdot}1$, $M = 220$ kg, length of shaft $= 0{\cdot}1016$ m, bearing length $= 0{\cdot}0508$ m, bearing diameter $= 0{\cdot}1016$ m, clearance $= 0{\cdot}000106$ M, viscosity of oil $= 0{\cdot}00568$, Ns/m^2.

the shaft. Under this situation a study has been carried out with the rotor disc kept at the center of the shaft.

Figure 16 shows the variation of DLIMIT with respect to the non-dimensional coefficient of internal damping. It is observed that an increase in internal damping force in the shaft reduces the stability limit speed of the system drastically.

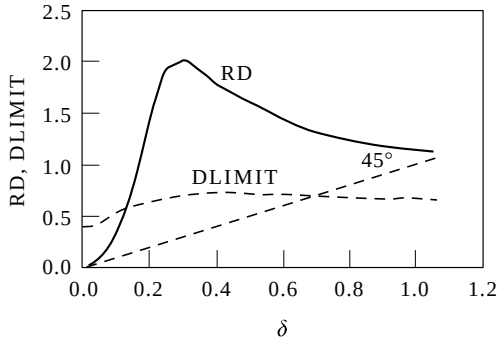

Figure 17. Variation of RD and DLIMIT w.r.t. δ when RD is minimized, with slope control.

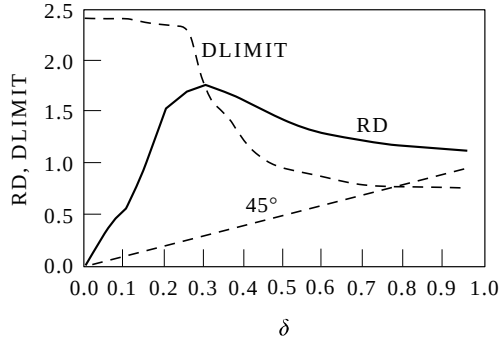

Figure 18. Variation of RD and DLIMIT w.r.t. δ when RD is minimized and DLIMIT is maximized, with slope control.

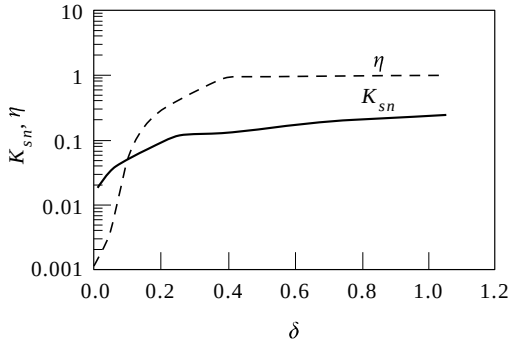

Figure 19. Variation of K_{sn} and η w.r.t. δ when RD is minimized, with slope control.

Figures 17 and 18 show the variation of RD and DLIMIT with respect to δ for Schemes I and II, respectively, with the concept of slope control imposed on the variation of support parameters. Figures 14 and 15 present the respective support characteristics. It is observed that Scheme II provides a higher stability limit speed in comparison to Scheme I. This happens because the destabilizing fluid film forces are not dependent on the amplitude of rotor response like the internal damping forces in the shaft. Hence, Scheme I works well as long as the

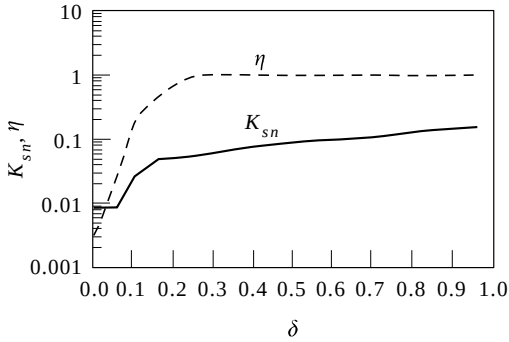

Figure 20. Variation of K_{sn} and η w.r.t. δ when RD is minimized and DLIMIT is maximized, with slope control.

destabilizing force depends on a rotor response, as in the case of a rotor–shaft system having rolling element bearings, but Scheme II proves more efficient otherwise. It is noted from Figures 19 and 20 that the support characteristics are smooth enough and do not involve any sudden changes.

A comparison of Figures 12, 13, 17 and 18 shows that Scheme II is certainly more useful in the case of a rotor–shaft system supported on journal bearings where destabilizing forces are also offered by fluid films in addition to the internal damping present in the shaft. Hence, the optimization process as in Scheme I may be followed for systems with rolling element bearings, whereas Scheme II is a must for systems with fluid film bearings.

7. CONCLUSIONS

From the work the following conclusions can be drawn.

Gyroscopic effect increases the stability limit speed of a system mounted on rolling element bearings.

Simultaneous minimization of the unbalance response amplitude and maximization of stability limit speed (Scheme II) proves more useful than only minimizing the unbalance response (Scheme I) for obtaining suitable frequency dependent support characteristics.

Optimization Scheme II is much more time consuming than Scheme I.

For getting a feasible support characteristic, slope control of support parameters is essential for the rotor-shaft system with both rolling element and hydrodynamic journal bearings.

As all the parameters have been non-dimensionalised, the results will be valid for any parametric value of a rotor–shaft system.

REFERENCES

1. J. W. LUND 1965 *Journal of Applied Mechanics, Transactions of ASME* Dec., **32**(4), 911–920. The stability of an elastic rotor in journal bearing with flexible damped supports.

2. E. J. GUNTER JR. and P. R. TRUMPLER 1969 *Journal of Engineering for Industry, Transactions of ASME* Nov., **91**(4), 1105–1113. The influence of internal friction on stability of high speed rotors with anisotropic supports.
3. R. G. KIRK and E. J. GUNTER 1972 *Journal of Engineering for Industry Transactions of ASME* Feb., **94**(1), 221–232. The effect of support flexibility and damping on the synchronous response of a single-mass flexible rotor.
4. J. W. LUND 1974 *Journal of Engineering for Industry* May, **96**(2), 509–517. Stability and damped critical speed of a flexible rotor in fluid film bearings.
5. W. D. PILKEY *et al*. 1976 *Journal of Engineering for Industry* Aug, **98**(3), 1026–1029. Efficient optimal design of suspension systems for rotating shafts.
6. R. B. BHAT, J. S. RAO and T. S. SANKAR 1982 *Journal of Mechanical Design Transactions of ASME* **104**, 339–344. Optimum journal bearing parameters for minimum rotor unbalance response in synchronous whirl.
7. L. E. BARRET *et al*. 1978 *Journal of Engineering for Power, Transactions of ASME* Jan., **100**(1), 89–94. Optimum bearing and support damping for unbalance response and stability of rotating machinery.
8. M. DARLOW and E. ZORZI 1981 *Mechanical Design Handbook for Elastomers. NASA*, CR 3423.
9. J. K. DUTT and B. C. NAKRA 1992 *Journal of Sound and Vibration* **153**, 89–96. Stability of rotor systems with viscoelastic supports.
10. J. K. DUTT and B. C. NAKRA 1993 *Journal of Vibration and Acoustics* **115**, 221–223. Vibration response reduction of a rotor shaft system using viscoelastic polymeric supports.
11. A. TONDL 1965 *Some Problems in Rotor Dynamics*. Prague: Publishing house of Czechoslovak Academy of sciences; seond edition.
12. B. S. GARBOW *et al*. 1977 *Lecturer Notes in Computer Science*, *Matrix Eigensystem Routines—EISPACK Guide Extension*, Berlin: Springer.
13. J. S. RAO 1985 *Mechanism and Machine Theory* **20**, 181–187. Instability of rotors mounted in fluid film bearings with a negative-cross coupled stiffness coefficient.
14. A. D. NASHIF, D. I. G. JONES and J. P. HENDERSON 1985 *Vibration damping*. New York: Wiley-Interscience.
15. S. S. RAO 1992 *Optimization Theory and Application*. Wiley Eastern Ltd.

APPENDIX A

$$M_2\ddot{X}_2 + K_sX_s - C_{12}(\phi - \beta) + C_i\dot{X}_s + C_i\omega Y_s = 0, \tag{A1}$$

$$M_2\ddot{Y}_2 + K_sY_s - C_{12}(\theta - \alpha) + C_i\dot{Y}_s - C_i\omega X_s = 0, \tag{A2}$$

$$(K_{xx})_L X_{JL} + (K_{xy})_L Y_{JL} - K_sX_se_2 - C_i\dot{X}_se_2 - C_i\omega Y_se_2 + (C_{xx})_L\dot{X}_{JL}$$

$$+(C_{xy})_L\dot{Y}_{JL} + C_{22}(\phi - \beta)/l + C_{12}(\phi - \beta)e_2 - (C_{12}X_s/l) = 0, \tag{A3}$$

$$(K_{yx})_L X_{JL} + (K_{yy})_L Y_{JL} - K_sY_se_2 - C_i\dot{Y}_se_2 + C_i\omega X_se_2 + (C_{yx})_L\dot{X}_{JL}$$

$$+(C_{yy})_L\dot{Y}_{JL} + C_{22}(\theta - \alpha)/l + C_{12}(\theta - \alpha)e_2 - C_{12}Y_s/l = 0, \tag{A4}$$

$$(K_{xx})_R X_{JR} + (K_{xy})_R Y_{JR} - K_s X_s e_1 - C_i \dot{X}_s e_1 - C_i \omega Y_s e_1 + (C_{xx})_R \dot{X}_{JR}$$

$$+(C_{xy})_R \dot{Y}_{JR} - C_{22}(\phi - \beta)/l + C_{12}(\phi - \beta)e_1 + C_{12} X_s/l = 0, \quad \text{(A5)}$$

$$(K_{yx})_R X_{JR} + (K_{yy})_R Y_{JR} - K_s Y_s e_1 - C_i \dot{Y}_s e_1 + C_i \omega X_s e_1 + (C_{yx})_R \dot{X}_{JR}$$

$$+(C_{yy})_R \dot{Y}_{JR} - C_{22}(\theta - \alpha)/l + C_{12}(\theta - \alpha)e_1 + C_{12} Y_s/l = 0, \quad \text{(A6)}$$

$$M_1 \ddot{X}_{1L} - K_s X_s e_2 + C_{22}(\phi - \beta)/l + K_1 X_{1L} + C_1 \dot{X}_{1L} + K_2(X_{1L} - X_{3L})$$

$$+C_{12}(\phi - \beta)e_2 - C_{12} X_s/l - C_i \dot{X}_s e_2 - C_i \omega Y_s e_2 = 0, \quad \text{(A7)}$$

$$M_1 \ddot{Y}_{1L} - K_s Y_s e_2 + C_{22}(\theta - \alpha)/l + K_1 Y_{1L} + C_1 \dot{Y}_{1L} + K_2(Y_{1L} - Y_{3L})$$

$$+C_{12}(\theta - \alpha)e_2 - C_{12} Y_s/l - C_i \dot{Y}_s e_2 + C_i \omega X_s e_2 = 0, \quad \text{(A8)}$$

$$M_1 \ddot{X}_{1R} - K_s X_s e_1 - C_{22}(\phi - \beta)/l + K_1 X_{1R} + C_1 \dot{X}_{1R} + K_2(X_{1R} - X_{3R})$$

$$+C_{12}(\phi - \beta)e_1 + C_{12} X_s/l - C_i \dot{X}_s e_1 - C_i \omega Y_s e_1 = 0, \quad \text{(A9)}$$

$$M_1 \ddot{Y}_{1R} - K_s Y_s e_1 - C_{22}(\theta - \alpha)/l + K_1 Y_{1R} + C_1 \dot{Y}_{1R} + K_2(Y_{1R} - Y_{3R})$$

$$+C_{12}(\theta - \alpha)e_1 + C_{12} Y_s/l - C_i \dot{Y}_s e_1 + C_i \omega X_s e_1 = 0, \quad \text{(A10)}$$

$$K_2(X_{3L} - X_{1L}) + C_2 \dot{X}_{3L} = 0, \quad \text{(A11)}$$

$$K_2(Y_{3L} - Y_{1L}) + C_2 \dot{Y}_{3L} = 0, \quad \text{(A12)}$$

$$K_2(X_{3R} - X_{1R}) + C_2 \dot{X}_{3R} = 0, \quad \text{(A13)}$$

$$K_2(Y_{3R} - Y_{1R}) + C_2 \dot{Y}_{3R} = 0, \quad \text{(A14)}$$

$$I_t \ddot{\phi} + C_{22}(\phi - \beta) + I_p \omega \dot{\theta} - C_{12} X_s = 0, \quad \text{(A15)}$$

$$I_t \ddot{\theta} + C_{22}(\theta - \beta) - I_p \omega \dot{\phi} - C_{12} Y_s = 0. \quad \text{(A16)}$$

APPENDIX B

$$\delta^2 x_2 + A_1 x_s - A_2(\phi' - x_{as}) + 2\zeta_i \delta x_s + 2\zeta_i \delta y_s = \delta^2, \quad \text{(B1)}$$

$$\delta^2 y_2 + A_1 y_s - A_2(\theta' - y_{as}) + 2\zeta_i \delta y_s - 2\zeta_i \delta x_s = -i\delta^2, \tag{B2}$$

$$(\beta_{xx})_L x_{JL} + (\beta_{xy})_L y_{JL} - A_1 e_2 x_s - 2\zeta_i \delta e_2 x_s - 2\zeta_i \delta e_2 y_s$$
$$+A_3(\phi' - x_{as}) + 2(\zeta_{xx})_L \delta x_{JL} + 2(\zeta_{xy})_L \delta y_{JL} + A_2(\phi' - x_{as})e_2 - A_2 x_s = 0, \tag{B3}$$

$$(\beta_{yx})_L x_{JL} + (\beta_{yy})_L y_{JL} - A_1 e_2 y_s - 2\zeta_i \delta e_2 y_s + 2\zeta_i \delta e_2 x_s$$
$$+A_3(\theta' - y_{as}) + 2(\zeta_{yx})_L \delta x_{JL} + (2\zeta_{yy})_L \delta y_{JL} + A_2(\theta' - y_{as})e_2 - A_2 y_s = 0, \tag{B4}$$

$$(\beta_{xx})_R x_{JR} + (\beta_{xy})_R y_{JR} - A_1 e_1 x_s - 2\zeta_i \delta e_1 x_s - 2\zeta_i \delta e_1 y_s + A_3(\phi' - x_{as})$$
$$+2(\zeta_{xx})_R \delta x_{JR} + 2(\zeta_{xy})_R \delta y_{JR} + A_2(\phi' - x_{as})e_1 + A_2 x_s = 0, \tag{B5}$$

$$(\beta_{yx})_R x_{JR} + (\beta_{yy})_R y_{JR} - A_1 e_1 y_s - 2\zeta_i \delta e_1 y_s + 2\zeta_i \delta e_1 x_s$$
$$-A_3(\theta' - y_{as}) + 2(\zeta_{yx})_R \delta x_{JR} + (2\zeta_{yy})_R \delta y_{JR} + A_2(\theta' - y_{as})e_1 + A_2 y_s = 0, \tag{B6}$$

$$\alpha_1 \delta^2 x_{1L} - A_1 e_2 x_s + A_3(\phi' - x_{as}) + \beta_1 x_{1L} + \beta_2(x_{1L} - x_{3L})$$
$$+2\zeta_1 \delta x_{1L} + A_2 e_2(\phi' - x_{as}) - A_s x_s - 2\zeta_i \delta e_2 x_s - 2\zeta_i \delta e_2 y_s = 0, \tag{B7}$$

$$\alpha_1 \delta^2 y_{1L} - A_1 e_2 y_s + A_3(\theta' - y_{as}) + \beta_1 y_{1L} + \beta_2(y_{1L} - y_{3L})$$
$$+2\zeta_1 \delta y_{1L} + A_2 e_2(\theta' - y_{as}) - A_2 y_s - 2\zeta_i \delta e_2 y_s + 2\zeta_i \delta e_2 x_s = 0, \tag{B8}$$

$$\alpha_1 \delta^2 x_{1R} - A_1 e_1 x_s - A_3(\phi' - x_{as}) + \beta_1 x_{1R} + \beta_2(x_{1R} - x_{3R})$$
$$+2\zeta_1 \delta x_{1R} + A_2 e_1(\phi' - x_{as}) + A_2 x_s - 2\zeta_i \delta e_1 x_s - 2\zeta_i \delta e_1 y_s = 0, \tag{B9}$$

$$\alpha_1 \delta^2 y_{1R} - A_1 e_1 y_s - A_3(\theta' - y_{as}) + \beta_1 y_{1R} + \beta_2(y_{1R} - y_{3R})$$
$$+2\zeta_1 \delta y_{1R} + A_2 e_1(\theta' - y_{as}) + A_2 y_s - 2\zeta_i \delta e_1 y_s + 2\zeta_i \delta e_1 x_s = 0, \tag{B10}$$

$$\beta_2(x_{3L} - x_{1L}) + 2\zeta_2 \delta x_{3L} = 0, \tag{B11}$$

$$\beta_2(y_{3L} - y_{1L}) + 2\zeta_2 \delta y_{3L} = 0, \tag{B12}$$

$$\beta_2(x_{3R} - x_{1R}) + 2\zeta_2 \delta x_{3R} = 0, \tag{B13}$$

$$\beta_2(y_{3R} - y_{1R}) + 2\zeta_2 \delta y_{3R} = 0, \tag{B14}$$

$$A_3\delta^2c^2\phi' + A_3(\phi' - x_{as}) + RA_3\delta^2c^2\theta' - A_2x_s = 0, \tag{B15}$$

$$A_3\delta^2c^2\theta' + A_3(\theta' - y_{as}) - RA_3\delta^2c^2\phi' - A_2y_s = 0, \tag{B16}$$

where $x_{as} = (x_{JR} + x_{1R} - x_{JL} - x_{1L})$, $y_{as} = (y_{JR} + y_{1R} - y_{JL} - y_{1L})$ $\phi' = \phi l$, $\theta' = \theta l$, $A_1 = (e_1^2 + e_2^2 - e_1e_2)/e_1e_2$, $A_2 = (e_1 - e_2)$ and $A_3 = e_1e_2$.

APPENDIX C: NOMENCLATURE

α	angular orientations of rotor axis about X-axis
β	angular orientations of rotor axis about Y-axis
C_1	primary support damping
C_2	secondary support damping
C_{mn}	fluid film damping coefficients for journal bearings [$m = x, y$; $n = x, y$]
C_i	internal damping coefficient
C_c	critical damping coefficient ($2M_2\omega_n$)
C_{12}	force/angular deflection or moment/deflection of the shaft at rotor disc location i.e., $K^*l(e_1 - e_2)$
C_{22}	moment/angular deflection or angular stiffness of the shaft at rotor disc location i.e., $K^*l^2(e_1e_2)$
$\cdot$	d/dt
D	dissipation energy
e_u	eccentricity at rotor disc
e_1 and e_2	l_1/l and l_2/l
E	Young's modulus of elasticity for shaft material
F	force vector
Q	displacement vector
f	amplitude of force
I_p and I_t	polar and transverse mass moments of inertia of the disc
i	$\sqrt{-1}$
K^*	$3EIl/(l_1^2l_2^2)$
$K_{support}$	$(K_1K_2 + i\omega(K_1C_2 + K_2C_1 + K_2C_2) - C_1C_2\omega^2)/(K_2 + i\omega C_2)$ is the complex support stiffness can also be written as $K_{sn}(1 + i\eta)$ where K_{sn} is in-phase support stiffness and η is the loss factor
K_b	stiffness of the rolling element bearing
K_1 and K_2	primary and secondary support stiffness
$K_{i,j}$	fluid film stiffness coefficients for journal bearing [$i = x, y$; $j = x, y$]
l_1 and l_2	distance of rotor disc from left and right bearing
l	length of the shaft
M_1 and M_2	mass of the support and mass of the rotor
t	time in seconds
T and V	kinetic and potential energy
θ	absolute angular deflections of rotor axis about X-axis
ψ	absolute angular deflections of rotor axis about Y-axis

ω	angular velocity of the rotor
ω_n	fundamental undamped natural frequency of the system $\sqrt{K^*/M_2}$

Non-dimensional terms

α_1	mass ratio (M_1/M_2)
β_b	non-dimensional bearing stiffness (K_b/K^*)
$(\beta_{ij})_k$	$(K_{ij})_k/K^*$ for $[i=x, y; j=x, y; k=L, R]$
$(\zeta_{ij})_k$	$(C_{ij})_k/C_c$ for $[i=x, y; j=x, y; k=L, R]$
DLIMIT	non-dimensional stability limit (stability limit speed ω)
δ	ω/ω_n i.e., the non-dimensional speed of rotation of the rotor disc
R	I_p/I_t
RD	non-dimensional response (i.e., $\lvert z_2\rvert/e_u$)
z_2	$[\text{Real}(x_2 e^{i\omega t}) + i\text{Real}(y_2 e^{i\omega t})]$
ζ_i	C_i/C_c

Support parameters

β_1 and β_2	K_1/K^* and K_2/K^*
ζ_1 and ζ_2	C_1/C_2 and C_c/C_c

Support characteristics

K_{sn}	non-dimensional in-phase support stiffness (i.e., $\text{Real}(K_{support})/K^*$)
η	loss factor of support and is given as $\text{Imag}(K_{support})/\text{Real}(K_{support})$